

Optimization-based conservative transport on the cubed-sphere grid

Kara Peterson¹, Pavel Bochev¹, and Denis Ridzal²

¹ Numerical Analysis and Applications,

² Optimization and Uncertainty Quantification,

Sandia National Laboratories³, Albuquerque, NM 87185-1320, USA,

{kjpeter,pbboche,dridzal}@sandia.gov

Abstract. Transport algorithms are highly important for dynamical modeling of the atmosphere, where it is critical that scalar tracer species are conserved and satisfy physical bounds. In this paper we present an optimization-based algorithm for the conservative transport of scalar quantities (*i.e.* mass) on the cubed sphere grid, which preserves monotonicity without the use of flux limiters. In this method the net mass updates to the cell are the optimization variables, the objective is to minimize the discrepancy between a high-order mass update (the “target”) and a mass update that satisfies physical bounds, whereas mass conservation is imposed by a single equality constraint. The resulting robust and efficient algorithm for conservative and monotone transport on the sphere further demonstrates the flexibility and scope of the recently developed optimization-based modeling approach [1, 2].

1 Introduction

In this paper we describe a conservative, and monotone optimization-based transport algorithm and its application to a cubed sphere grid. The method is based on an incremental remap approach [3] with an optimization-based remap step at the core. The efficient mass variable mass target (MVMT) algorithm [4] is used for the remap step. In this approach a high-order mass update is used as the target for the optimization and monotonicity and mass conservation are guaranteed through the constraints.

Numerical results are shown for standard transport tests on the sphere. An incremental remap transport algorithm in which the remap step is implemented using the flux-corrected remap (FCR) [5] provides a benchmark for the numerical studies. The studies show that the optimization-based algorithm is computationally competitive with the benchmark and is more robust in the case of complex flows.

³ Sandia National Laboratories is a multi-program laboratory managed and operated by Sandia Corporation, a wholly owned subsidiary of Lockheed Martin Corporation, for the U.S. Department of Energy’s National Nuclear Security Administration under contract DE-AC04-94AL85000.

2 Optimization-based MVMT Transport

We briefly review the MVMT optimization-based transport algorithm for the scalar transport problem

$$\frac{\partial \rho}{\partial t} + \nabla \cdot \rho \mathbf{v} = 0 \quad \text{on } \Omega \times [0, T] \quad \text{and} \quad \rho(\mathbf{x}, 0) = \rho^0(\mathbf{x}) \quad (1)$$

while conserving mass and maintaining monotonicity and positivity. To achieve conservative and monotone numerical solution we use an incremental remapping approach [3] with an optimization-based framework for the remap step [6, 4, 7].

Consider a partition $C(\Omega)$ of Ω into cells $c_i, i = 1, \dots, C$. We define the cell mass to be $m_i = \int_{c_i} \rho(\mathbf{x}, t) dV$ and the cell measure to be $\mu_i = \int_{c_i} dV$. In the incremental remapping transport algorithm, the cell average density defined as $\rho_i = m_i/\mu_i$, is the primary quantity of interest. The algorithm is motivated by the fact that mass is conserved within Lagrangian volumes and cell average density depends only on the constant mass and the updated Lagrangian volume measure. Given a grid configuration $C(\Omega(t))$, cells masses ($m_i(t)$), cell areas ($\mu_i(t)$), and cell average densities ($\rho_i(t)$) at time t the incremental remapping algorithm consists of three steps:

1. Project the grid at time t to an arrival grid at time $t + \Delta t$ using the velocity field: $C(\Omega(t)) \mapsto C(\Omega(t + \Delta t))$;
2. Update to mass and cell average density after the Lagrangian step: $m_i(t + \Delta t) = m_i(t)$, $\rho_i(t + \Delta t) = m_i(t)/\mu_i(t + \Delta t)$ for $i = 1, \dots, C$;
3. Remap cell average density to departure grid \tilde{C} : $m(t + \Delta t) \mapsto \tilde{m}$ and $\rho(t + \Delta t) \mapsto \tilde{\rho}$, for $i = 1, \dots, C$.

In the final remap step the mean density values on the Lagrangian grid $\rho_i(t + \Delta t)$ are used to find approximations of the new masses \tilde{m}_i and mean densities $\tilde{\rho}_i$ on the departure grid. The remapped values should satisfy conservation of mass and local bounds. This step can be formulated as an optimization problem where we define a target quantity (u^\top) that is a function of a stable and accurate density solution to the transport problem in Eq. (1), but may not be conservative or satisfy local bounds. We minimize the distance between our solution \hat{u} and the target with the constraints of mass conservation and local bounds preservation. This ensures that the solution is globally optimal with respect to the target and the desired physical properties. This MVMT formulation can be written as

$$\begin{cases} \text{minimize} & \frac{1}{2} \|\hat{u} - u^\top\|_{\ell_2}^2 & \text{subject to} \\ \hat{u} \in C^h; & \sum_{i=1}^C \hat{u}_i = 0 & \text{and} \quad \tilde{m}^{\min} \leq m + \hat{u} \leq \tilde{m}^{\max} \end{cases} \quad (2)$$

where C^h is the piecewise constant space with respect to cells.

The target in each cell is defined to be the difference between the mass in the final configuration \tilde{c}_i and the Lagrangian cell c_i

$$u_i^\top := \int_{\tilde{c}_i} \rho^h(\mathbf{x}) dV - \int_{c_i} \rho^h(\mathbf{x}) dV; \quad i = 1, \dots, C \quad (3)$$

for the following mean preserving linear density reconstruction

$$\rho^h(\mathbf{x})|_{c_i} = \rho_i + \mathbf{g}_i \cdot (\mathbf{x} - \mathbf{b}_i) \quad (4)$$

where

$$\mathbf{g}_i \approx \nabla \rho \quad \text{and} \quad \mathbf{b}_i = \frac{\int_{c_i} \mathbf{x} dV}{\mu_i}. \quad (5)$$

In practice, the approximation to the gradient of the density (\mathbf{g}) is obtained by a least-squares fit that employs the cell averaged density in neighboring cells. The target mass increment is computed by integrating the density reconstruction over the intersections of the old (Lagrangian) mesh with the new mesh. Rather than computing exact intersections we use a swept region approximation [6, 7].

3 Extension of MVMT Transport to cubed sphere grid

The cubed sphere grid, originally introduced by Sadournay [8], consists of six faces or panels of a cube that are projected onto the surface of a sphere. This configuration avoids the pole singularity that plagues latitude/longitude grids and is in increasing use among the climate community. To define the grid partition we use an equiangular gnomonic projection where $\alpha, \beta \in [-\pi/4, \pi/4]$ are central angles, which can be related to the local panel coordinates x_p, y_p by

$$x_p = a \tan \alpha \quad y_p = a \tan \beta \quad p = 1, \dots, 6. \quad (6)$$

The coefficient a is related to the radius of the sphere R as $a = R/\sqrt{3}$. A plot of the six cube panels and an example cubed sphere grid are shown in Figure 1. Mappings between latitude/longitude coordinates and the cubed sphere coordinates can be found in [9].

Extension of the MVMT algorithm to a cubed-sphere grid requires modifications to the target computation, but does not in any way affect the definition of the constraints or the optimization algorithm. This is one of the key advantages of the optimization-based approach, which has been exploited in [?]

To compute the target mass increment the area integrals and linear density reconstruction must be reformulated for the cubed sphere curvilinear coordinates. In the incremental remap approach the area integrals are generally converted to line integrals via Green's theorem. Using Green's theorem with the nonorthogonal curvilinear cubed sphere panel coordinates, the area integral over a cell can be expressed as

$$\mu_i = \int_{c_i} dV = - \int_{\partial c_i} \frac{y_p}{r_p(1+x_p^2)} dx_p, \quad (7)$$

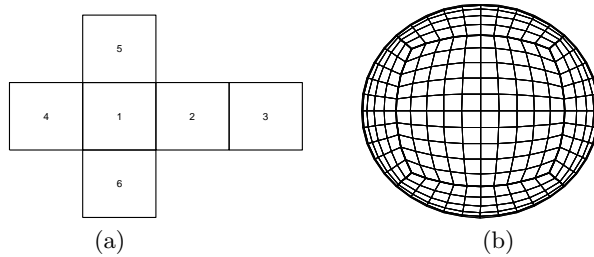


Fig. 1. (a) The six cube panels. (b) A sample cubed-sphere grid with 10x10 elements per panel.

The linear density reconstruction additionally requires barycenters of cells, which can be similarly written as

$$b_{x_i} = \frac{1}{\mu_i} \int_{c_i} x_p dV = -\frac{1}{\mu_i} \int_{\partial c_i} \frac{x_p y_p}{r_p (1 + x_p^2)} dx_p, \quad (8)$$

and

$$b_{y_i} = \frac{1}{\mu_i} \int_{c_i} y_p dV = -\frac{1}{\mu_i} \int_{\partial c_i} \frac{1}{r_p} dx_p. \quad (9)$$

Using these expressions, the mean preserving density reconstruction on the cubed sphere grid for a position \mathbf{s} on a panel p is

$$\rho^h(\mathbf{s})|_{c_i} = \rho_i + g_i^{x_p}(x_p - b_{x_i}) + g_i^{y_p}(y_p - b_{y_i}). \quad (10)$$

Once this density reconstruction is determined the MVMT algorithm as described in [4, 7] can be applied.

4 Results

To test the formulation on the cubed sphere grid, two standard test cases for transport on the sphere described in [10, 11] are used. In Example 1, we compute the solid body rotation of a Gaussian distribution on the sphere to test the convergence rate of the algorithm for the cubed sphere geometry. The temporally constant zonal flow field is given in terms of zonal (u) and meridional (v) components of the velocity on a sphere with longitude (λ) and latitude (θ) as

$$\begin{aligned} u(\lambda, \theta) &= 2\pi (\cos(\theta) \cos(\alpha) + \cos(\lambda) \sin(\theta) \sin(\alpha)) \\ v(\lambda, \theta) &= 2\pi \sin(\lambda) \sin(\alpha). \end{aligned} \quad (11)$$

The rotation angle α provides the orientation of the flow. For this test α is taken to be $\pi/4$, which is the most demanding orientation for the cubed-sphere geometry because the density distribution is transported over four of the corners of the cubed-sphere grid. The smooth Gaussian density distribution is initially

centered at $(\lambda_1, \theta_1) = (3\pi/2, 0)$ and is defined in terms of three-dimensional Cartesian coordinates (X, Y, Z) as

$$\rho(\lambda, \theta) = \exp(-5((X - X_1)^2 + (Y - Y_1)^2 + (Z - Z_1)^2)) \quad (12)$$

where $X_1 = \cos \lambda_1 \cos \theta_1$, $Y_1 = \sin \lambda_1 \cos \theta_1$, and $Z_1 = \sin \theta_1$.

Three grids are used with 30×30 , 60×60 , and 120×120 elements per panel corresponding to resolutions of 3° , 1.5° , and 0.75° along the equator. Results are computed using the incremental remapping approach discussed in Section 2 with the MVMT algorithm used for the remap step. For comparison results for FCR are given. At the final time the density distribution returns to the initial position, which allows for an error analysis. L_1 errors are computed as in [11].

Solid-body translation on the sphere (timings and L_1 error)

mesh	# steps	FCR		MVMT		FCR		MVMT	
		time(sec)	time(sec)	L_1 error	rate	L_1 error	rate		
3°	240	18.1	17.6	1.33e-2	—	1.49e-2	—		
1.5°	480	108.5	109.3	2.43e-3	2.45	2.65e-3	2.50		
0.75°	960	816.5	811.0	5.17e-4	2.34	5.44e-4	2.39		

Table 1. (1) Comparison of the computational costs of FCR and MVMT-a as measured by MatlabTM wall-clock times in seconds, on a single Intel Xeon X5450 3.0GHz processor, for the slotted-cylinder translation test on the sphere. (2) Comparison of the L_1 errors with respect to the initial condition.

Timings as well as L_1 errors and rates for the MVMT and FCR solutions are given in Table 1. For this simple translation of a smooth density distribution it is expected that MVMT and FCR perform similarly. Slightly better than second-order convergence is seen for both methods and the absolute errors are comparable. The computational costs of MVMT and FCR are virtually identical, owing to the efficiency of the MVMT optimization scheme. Plots of the density distribution at the initial time, at time $t = 0.15$ as the Gaussian hill is passing over a cubed sphere corner, and at the final time $t = 1$ are shown in Figure 2.

Example 2 is more demanding with an initial density distribution consisting of two notched cylinders with radius $r = 1/2$, height $h = 1$, and initial positions $(\lambda_1, \theta_1) = (5\pi/6, 0)$ and $(\lambda_2, \theta_2) = (7\pi/6, 0)$. Given the great circle distance between an arbitrary point (λ, θ) and a cylinder center (λ_i, θ_i)

$$r_i(\lambda, \theta) = \arccos(\sin \theta_i \sin \theta + \cos \theta_i \cos \theta \cos(\lambda - \lambda_i)), \quad (13)$$

the initial configuration of the notched cylinders may be expressed in latitude-longitude coordinates as

$$\rho(\lambda, \theta) = \begin{cases} h & \text{if } r_i < r \text{ and } |\lambda - \lambda_i| \geq r/6 \text{ for } i = 1, 2 \\ h & \text{if } r_1 < r \text{ and } |\lambda - \lambda_0| < r/6 \text{ and } \theta - \theta_0 < -5r/12 \\ h & \text{if } r_2 < r \text{ and } |\lambda - \lambda_1| < r/6 \text{ and } \theta - \theta_1 > 5r/12 \\ 0 & \text{otherwise.} \end{cases}$$

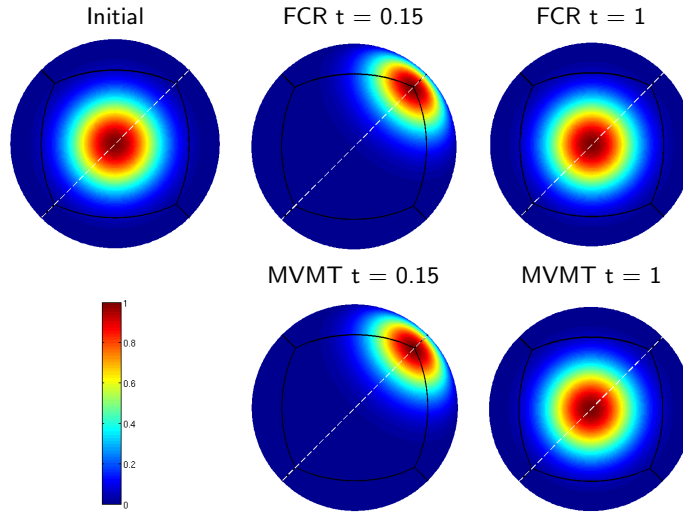


Fig. 2. Transport results for the solid-body rotation test on the sphere at the time the center of the density distribution passes over a cubed sphere corner ($t=0.15$) and at the final time ($t=1$) after one revolution (960 time steps) on a mesh with 120×120 elements per panel. The rotation angle of $\pi/4$ determines the trajectory shown on the plots as a white dashed line.

The cylinders are transported in the following deformation flow field with superimposed rotation

$$\begin{aligned} u(\lambda, \theta, t) &= 2 \sin^2(\lambda - 2\pi t/T) \sin(2\theta) \cos(\pi t/T) + 2\pi \cos(\theta)/T \\ v(\lambda, \theta, t) &= 2 \sin(2(\lambda - 2\pi t/T)) \cos(\theta) \cos(\pi t/T) \end{aligned} \quad (14)$$

where the period T is set to 5.

Timings as well as L_1 errors and rates for the MVMT and FCR solutions are given in Table 2 and plots of the density distribution at the initial time, at a time of maximum deformation $t = 2.5$ and a final time $t = 5$ are shown in Figure 3. Second-order convergence is not seen for either method in this case due to the discontinuous density field, but the errors and convergence rates appear comparable. Note, however that the FCR solution has a minimum value of -0.0639 and a maximum value of 1.075 , while the MVMT solution remains within the physical bounds $[0, 1]$. If the number of time steps is decreased to 1650, which corresponds to a maximum Courant-Friedrichs-Lewy (CFL) number of 0.985, the FCR solution blows up, but the MVMT solution still remains monotone and appears reasonable visually (Figure 4).

5 Conclusion

A computationally efficient optimization-based transport algorithm detailed in [4, 7] has been modified for the cubed sphere geometry. The resulting formula-

Deformational transport on the sphere (timings and L_1 error)

mesh	# steps	FCR		MVMT		FCR		MVMT	
		time(sec)	time(sec)	L_1 error	rate	L_1 error	rate	L_1 error	rate
3°	600	45.9	45.0	9.38e-1	—	9.54e-1	—		
1.5°	1200	274.1	277.5	6.17e-1	0.60	6.53e-1	0.55		
0.75°	2400	2081.0	2071.5	4.16e-1	0.59	4.45e-1	0.55		

Table 2. (1) Comparison of the computational costs of FCR and MVMT as measured by MatlabTM wall-clock times in seconds, on a single Intel Xeon X5450 3.0GHz processor, for the nondivergent deformational velocity test on the sphere. (2) Comparison of the L_1 errors with respect to the initial condition.

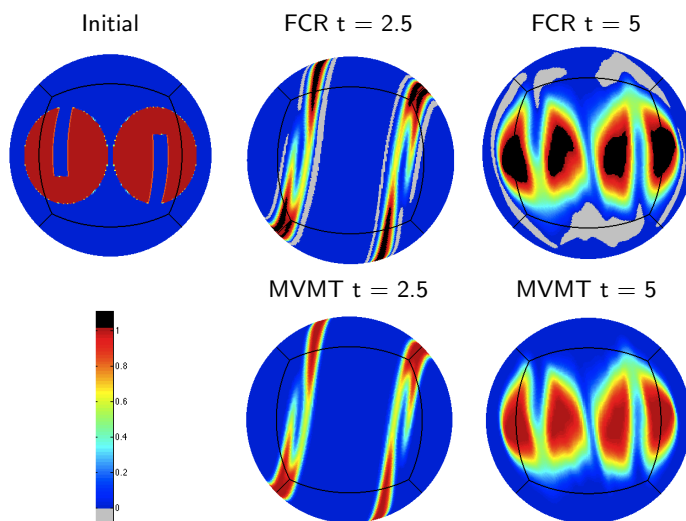


Fig. 3. Transport results for the nondivergent deformational flow test on the sphere, shown at the time of maximum deformation ($t = 2.5$) and at the final time ($t = 5$) for a total of 2400 time steps on a mesh with 120×120 elements per panel.

tion has been tested on two standard transport cases for the sphere [12]. The optimization-based transport is shown to be computationally competitive with an algorithm based on flux-corrected remap and to exhibit similar errors for the simplest test case. For the more challenging test case MVMT maintains positivity and is more robust for larger time steps.

References

1. Bochev, P., Ridzal, D., Scovazi, G., Shashkov, M.: Constrained optimization based data transfer – a new perspective on flux correction. In Kuzmin, D., Lohner, R., Turek, S., eds.: Flux-Corrected Transport. Principles, Algorithms and Applications. 2nd edn. Springer Verlag, Berlin, Heidelberg (2012) 345–398

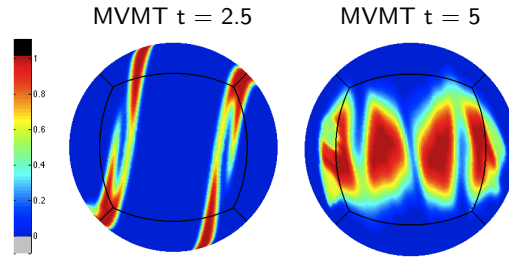


Fig. 4. Transport results for the nondivergent deformational flow test with rotation on the sphere, shown at the time of maximum deformation ($t = 2.5$) and at the final time ($t = 5$) for a total of 1650 time steps for a maximum CFL number of 0.985 on a mesh with 120×120 elements per panel. The FCR solution blows up for this long time step case and is therefore not shown.

2. Bochev, P., Ridzal, D., Young, D.: Optimization-based modeling with applications to transport. Part 1. Abstract formulation. In Lirkov, I., Margenov, S., Wasniewski, J., eds.: Proceedings of LSSC 2011. Springer Lecture Notes in Computer Science (Submitted 2011)
3. Dukowicz, J.K., Baumgardner, J.R.: Incremental remapping as a transport/advection algorithm. *J. Comput. Phys.* **160**(1) (2000) 318 – 335
4. Bochev, P., Ridzal, D., Shashkov, M.: Fast optimization-based conservative remap of scalar fields through aggregate mass transfer. *J. Comput. Phys.* **Submitted** (2012)
5. Liska, R., Shashkov, M., Váchal, P., Wendroff, B.: Optimization-based synchronized flux-corrected conservative interpolation (remapping) of mass and momentum for arbitrary Lagrangian-Eulerian methods. *J. Comput. Phys.* **229** (March 2010) 1467–1497
6. Bochev, P., Ridzal, D., Scovazzi, G., Shashkov, M.: Formulation, analysis and numerical study of an optimization-based conservative interpolation (remap) of scalar fields for arbitrary lagrangian-eulerian methods. *J. Comput. Phys.* **230**(13) (2011) 5199 – 5225
7. Bochev, P., Ridzal, D., Peterson, K.: Optimization-based remap and transport: a divide and conquer strategy for feature-preserving discretizations. *J. Comput. Phys.* **Submitted** (2013)
8. Sadournay, R.: Conservative finite-differencing approximations of the primitive equations on quasi-uniform spherical grids. *Monthly Weather Review* **100** (1972) 136–144
9. Nair, R.D., Thomas, S.J., Loft, R.D.: A discontinuous Galerkin transport scheme on the cubed sphere. *Monthly Weather Review* **133** (2005) 814–828
10. Nair, R.D., Lauritzen, P.H.: A class of deformational flow test cases for linear transport problems on the sphere. *J. Comput. Phys.* **229** (2010) 8868–8887
11. Lauritzen, P.H., Skamarock, W.C., Prather, M.J., Taylor, M.A.: A standard test case suite for two-dimensional linear transport on the sphere. *Geosci. Model Dev. Discuss.* **5** (2012) 189–228
12. Lauritzen, P.H., Nair, R.D., Ullrich, P.A.: A conservative semi-lagrangian multi-tracer transport scheme (cslam) on the cubed-sphere grid. *J. Comput. Phys.* **229** (2010) 1401–1424